Analyst

Flexible thread-based electrochemical sensor for oxygen monitoring

Journal:	*Analyst*
Manuscript ID	AN-ART-12-2020-002400.R1
Article Type:	Paper
Date Submitted by the Author:	26-Feb-2021
Complete List of Authors:	Xia, Junfei; Tufts University, Department of Electrical and Computer Engineering Sonkusale, Sameer; Tufts University, Department of Electrical and Computer Engineering

Flexible thread-based electrochemical sensor for oxygen monitoring

Junfei Xia[a,b], Sameer Sonkusale[a,b*]

a Department of Electrical and Computer Engineering, Tufts University, Medford, MA, 02155
b Nano Lab, Advanced Technology Laboratory, Tufts University, Medford, MA, 02155

*Corresponding author

Abstract

Oxygen plays a key role in human physiology and is abnormally modulated in various disease pathologies making its in situ monitoring quite important. Most oxygen sensors are not able to measure oxygen levels deep inside the tissue or have a mismatched electrode-tissue interface. In this study we developed a flexible thread-based oxygen sensor that combines the unique advantages of minimal invasiveness and superior flexibility offering the possibility for tissue integration. The sensor is featured by a simple and low-cost fabrication approach which allows for measuring overall oxygen concentration either over a large surface area or locally at any spot in any three-dimensional environment with high spatial accuracy and high sensitivity. The sensor can sensitively detect dissolved oxygen levels within the physiological range of tissue oxygenation. The sensor's performance is insensitive to pH variation from 5.8 to 8.0. The sensor shows good repeatability and stability over a period of one week in phosphate buffered saline. In addition, the signal variation is less than 10% after hundreds of cycles of physical bending. Using a hydrogel-based tissue model the sensor has been shown to probe dissolved oxygen levels at different spatial locations inside a tissue-like environment.

Keywords: Thread diagnostics, oxygen sensor, electrochemical sensing, tissue oxygenation

1. Introduction

Oxygen plays a pivotal role in the human body for energy production through cellular respiration. It participates in a variety of bodily functions ranging from memory storage and cognitive function, to tissue repair and regeneration during wound healing.[1-4] The lack of oxygen supply in tissue or blood (termed hypoxia or hypoxemia) is associated with many diseases such as cerebral ischemia, congestive heart failure, and cancer.[5-7] While the level of oxygen has been shown to vary within different locations of the body, it can be used as a biomarker in assessing insufficient oxygen delivery and the resulting tissue damage.[8] More importantly, the monitoring of oxygen level directly supports the diagnosis and prognosis of hypoxia and hypoxemia-related diseases.

A plethora of methods have been proposed to evaluate tissue oxygenation. The optical-based oxygen sensors such as pulse oximetry have been routinely used for measuring oxygen saturation.[9] In recent years the development of fluorescent nanosensors has enabled intracellular sensing and imaging of oxygen with significantly enhanced spatial resolution.[10, 11] Despite the fast readout, 2-D mapping capability, and non-invasiveness of optical approaches,[12-14] they are often limited to superficial measurement due to the light attenuation within the tissue. The use of near-infrared light could enhance the tissue penetration depth but is still ineffective for probing oxygen deep inside the body such as in case of deep tissue injury.[15, 16] In addition, the superficial oxygen level could equilibrate with the atmospheric oxygen thus making the measurement less accurate. As an alternative, electrochemical oxygen sensor offers unparalleled temporal resolution, high sensitivity, and the capability of long-distance signal transmission when coupled with a wireless readout module.[17, 18] Tissue pO_2 has been measured using miniaturized metal-based micro-electrodes. For example, a recessed polarographic microcathode was fabricated to measure intracellular pO_2.[19-21] Traditional Clark-type electrode was also employed in sensing blood oxygen by placing an oxygen-sensitive cathode into a catheter that can be inserted into blood vessels.[22] A needle-type electrode was inserted subcutaneously for measuring wound oxygen tension in postoperative surgical patients.[23] Despite the high accuracy and sensitivity of microelectrodes, they are intrinsically flawed with the mismatch in mechanical attributes between rigid sensor and soft tissue, which could negatively impact the subject being measured. In addition, these electrodes often require invasive operations such as surgery to be implanted, and the lack of spatial resolution is a major limitation compared to optical methods.

Textile fabrics have been proposed to build point-of-care biosensors due to their natural conformability with human body, mechanical stability and durability, and low-cost fabrication processes.[24-26] Thread-based electrochemical sensors are of particular interests due to the cleanroom-free fabrication, large surface area for analyte interfacing, and wicking property for spontaneous sampling.[27] Thread-based

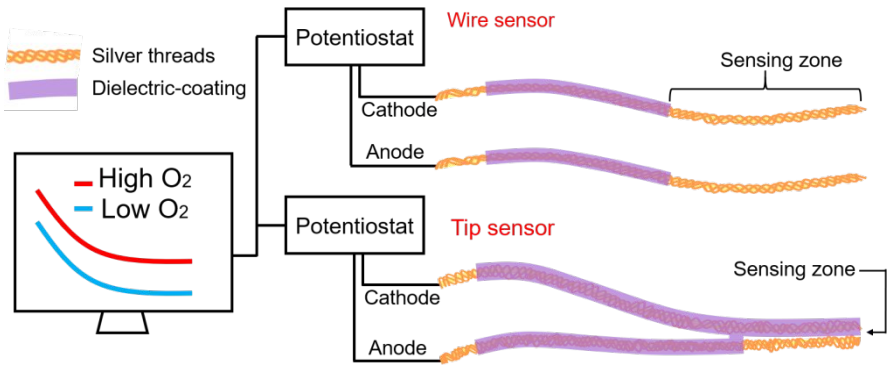

Figure 1. Schematic of two different thread-based electrochemical oxygen sensor: a wire-type sensor where the sensing zone is along the thread surface area. a tip-type sensor where the sensing zone is located at the tip region.

electrodes are more amenable to tissue microenvironment than rigid metal electrodes; they can be easily placed inside tissue using a suture needle, which allows for deep tissue measurement. Our group has previously engineered a textile-based electrochemical sensor for three-dimensional pH-sensing in the wound tissue and a thread-based electrochemical for sweat sensing.[27-29] In the current study we aim to develop an oxygen sensor by building it entirely from single thread/bundles that can either measure averaged oxygen level over a large surface area or 'pin-point' region of interest (ROI) to measure local oxygen level (**Figure 1**). We develop a novel fabrication approach for the 'tip' sensor where the sensing zone is confined at the tip of the thread to allow for precise local point measurement. We demonstrate the sensor can respond to different levels of oxygen in buffer solutions and can withstand mechanical deformation with minimum change in signal. In addition, we use a hydrogel-based tissue model to validate the sensor's performance.

2. Material and Methods

2.1 Reagents

Conductive silver thread (Liberator® 40) was purchased from Syscom Advanced Materials (Columbus, OH, USA). UV-curable dielectric ink was purchased from Kayaku Advanced Materials (Westborough, MA, USA). Agarose, potassium chloride (>99.0%), sodium phosphate monobasic (>99.0%), sodium phosphate dibasic (>99.0%), Dulbecco's Modified Eagle's Medium (DMEM) with high glucose were purchased from Sigma Aldrich (St. Louis, MO, USA). Phosphate buffers saline (PBS, pH 7.4), Fetal bovine serum (FBS) were purchased from Thermo Fisher Scientific (Waltham, MA, USA). Polyethylene terephthalate (PET) sheet was purchased from Amazon (seller: PP OPOUNT).

2.2 Sensor fabrication

In this work we developed two types of thread-based sensor: 'wire' type sensor and 'tip' type sensor. The fabrication process is schematically shown in **Figure 2**. The silver-coated thread was cleaned by sonicating in isopropyl alcohol (IPA) and distilled water (diH_2O) for 5 min, respectively. For making wire sensor, dielectric ink was coated on the middle portion of the thread and ~ 2 cm

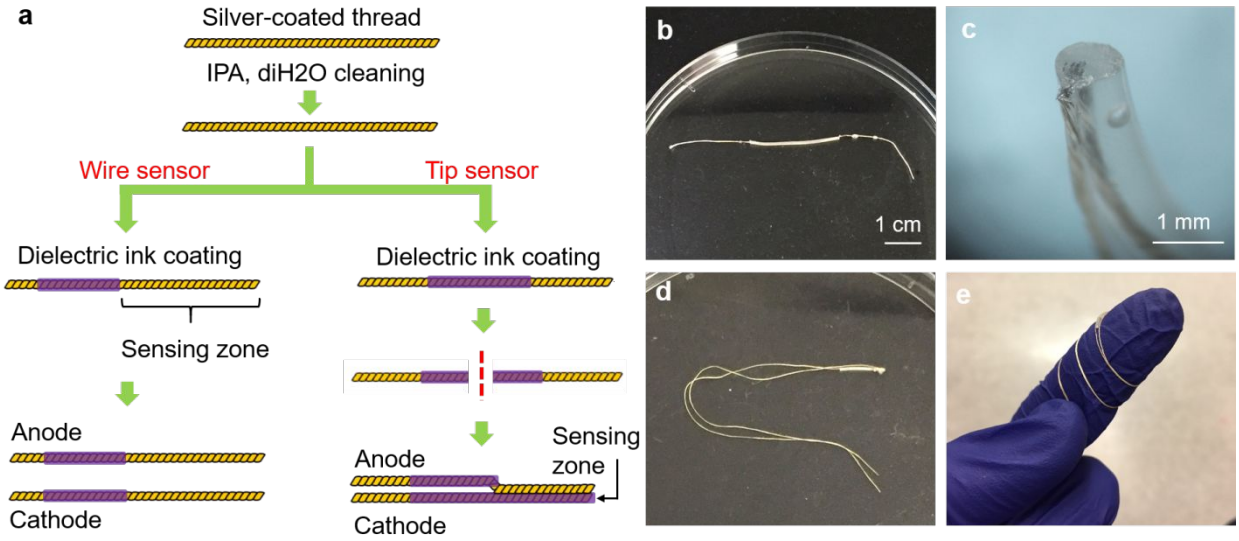

Figure 2. a) Schematic of fabrication procedure of thread-based oxygen sensor. Purple indicates dielectric coating. b) Photograph of a wire sensor (only one thread electrode is shown). c) Photograph of a tip sensor at the tip region. d) Photograph of a curved tip sensor. e) Photograph of a tip sensor looped around the finger.

segment was left uncoated as the sensing zone. The dielectric ink was cured under UV illumination. Two identical threads were fabricated in this manner as anode and cathode. For making the tip sensor, after dielectric coating and curing, the thread was cut in the middle to expose the cross-section of silver thread (**Figure 2a**). The cross-section area was used as the cathode for sensing oxygen. Another silver thread was bundled together at the tip region as the anode (**Figure 2c**). To control the thickness of dielectric coating as it affects the distance between two thread electrodes, a segment of polyvinyl chloride tube with inner diameter of 1 mm was used as a template to hold the dielectric ink during coating. The typical diameter of the tip is ~ 1 mm. It can be further reduced by reducing thickness of the dielectric coating. The fabricated thread-based sensors show good flexibility (**Figure 2d&e**).

2.3 Sensor calibration

The sensors were calibrated in PBS (pH 7.4, temperature 20.2 ˚C) with different concentrations of dissolved oxygen. For wire sensor, the distance of two thread electrodes is kept at 2 cm for all measurement. To adjust dissolved oxygen concentration, the sensing zone was soaked in PBS which was bubbled by a gas flow of oxygen/nitrogen mixture controlled by a gas blender (MCQ Instruments, Rome, Italy) for at least 5 min before measurement. Another commercial oxygen probe (Ocean Insight, Orlando, FL, USA) was used to determine dissolved oxygen concentrations in the PBS for calibration purpose. A potentiostat (CH Instrument, Austin, TX, USA) was used to measure the current response from the thread electrodes using two-electrode configuration by applying a biased potential of 0.55V relative to the silver cathode.

2.4 Interference study

Phosphate buffers with different pH were prepared by mixing 0.2M dibasic sodium phosphate and 0.2M monobasic sodium phosphate at different ratios. Potassium chloride was added into each buffer at a final concentration of 0.1M. The pH of home-made buffer was validated using a commercial pH probe (OAKTON Instruments, Vernon Hills, IL, USA). Both types of sensor were sequentially soaked in buffers with pH of 7.4, 5.8, 6.6, 8.0 for 20 min respectively, before the output signal was measured. Both types of sensor were then soaked in DMEM medium supplemented with 5% FBS for 20 min and the signal was recorded. Oxygen concentration was kept constant for all measurements (air-saturation).

2.5 Bending test

To test whether sensor's response is affected by mechanical deformation (i.e., bending), two silver threads were sewed parallelly onto a flexible PET sheet (2 cm × 3 cm) with their ends fixed using resin. The spacing between two threads was kept at 1 cm. Bending of the threads was achieved by bending the PET sheet. Threads were straightened before bending to make sure there was minimum change in distance between two threads during bending. The threads were soaked in air-saturated PBS and the current response was recorded when the sheet was bent at different degree. To mimic possible mechanical wear and tear, PET sheet was manually bent for 250 times and the sensor's response was compared with that before bending.

2.6 Repeatability and stability test

For repeatability test, the concentration of dissolved oxygen was changed by bubbling PBS with alternating nitrogen and air flow for 5 cycles. For stability test, the sensor was soaked in air-saturated PBS and air-saturated DMEM medium supplemented with 5% FBS for 7 days. The output current was measured every 24 hr for both types of sensor.

2.7 Tissue model

Agarose gel was used as a tissue phantom. 2% Agarose was dissolved in PBS with pH of 7.4. Four tip sensors (pre-calibrated) were inserted and fixed inside a 15 mL centrifuge tube from pre-drilled holes on the sidewall. Agarose solution was added into the tube and allowed to gel at room temperature. The cone-shaped bottom of the tube was cut to expose to open atmosphere. The empty space on the other side of the gel was filled with nitrogen by a constant nitrogen flow (flow rate: 40 mL/min) to establish an oxygen gradient across the gel. The nitrogen flow was kept for 30 min before the measurement to allow oxygen gradient to reach equilibrium.

3. Results and Discussion

3.1 Design of thread-based oxygen sensor

The thread-based electrochemical sensor uses two silver-coated thread as the cathode and anode. Under a constant polarizing potential, the following electrode reactions take place,

$$\text{Anode: } 4\,Ag + 4\,Cl^- \rightarrow 4\,AgCl + 4\,e^-$$

$$\text{Cathode: } 4\,H^+ + 4\,e^- + O_2 \rightarrow 2\,H_2O$$

$$\text{Overall: } 4\,Ag + 4\,Cl^- + 4H^+ + O_2 \rightarrow 4\,AgCl + 2\,H_2O$$

The resulting current passing through the cathode is in proportion to the dissolved oxygen concentration, which can be measured by amperometry techniques. We firstly applied a linear voltage scan between two electrodes in order to determine the suitable polarizing potential. As shown in **Figure S1**, the current difference between nitrogen-saturated and air-saturated samples increases as the voltage increases from 0 to 1V. We chose 0.55V as a reasonable polarization voltage as a significant difference in current was observed at this voltage. In traditional oxygen sensors, cathode is usually made of platinum or gold due to their superior stability.[30] However, it remains challenging to uniformly coat the threads with platinum or gold in a cost-effective manner. In this work silver is selected as a surrogate because it's relatively stable and has been used as cathode in oxygen sensors.[31] We noticed the color of anode thread changes from light yellow to dark yellow after several measurements, indicating the formation of silver chloride that precipitates on the surface of electrodes (**Figure S2**).[32] We found such precipitates did not affect the performance of wire sensor but had a significant impact on tip sensor when we used cross-section of the thread as both anode and cathode in the original design. The tip sensor failed to respond to high level of oxygen and became completely insensitive to oxygen afterwards (**Figure S3**) due to the complete coverage of electrode surface by AgCl precipitation. In contrast, the wire sensor was kept running for 80 min in air-saturated PBS without significant drift in current response (**Figure S4**). In order to increase the surface area of anode (which is also a typical electrode design to maintain a larger anode than cathode), we bundled a silver thread around the cathode thread so that the sensing zone is still at the tip (cathode) for sensing local oxygen concentration. The silver-coated thread is directly exposed to sensing environment for fast response. Non-specific interactions between electrode surface and biomolecules (such as adhesion of proteins) in the biological environment may hinder the electron transfer process and cause the sensor to

malfunction with increased contact time. Coating the thread surface with an hydrogel layer could potentially extend the working lifetime of the sensor in the biological environment.[33, 34]

3.2 Measurement of dissolved oxygen concentration in buffer solution

Next we calibrated the sensor by soaking the sensing zone in solutions with different concentrations of dissolved oxygen. In a traditional Clark electrode, the anode and cathode are soaked in a bath containing potassium chloride which provides the path for current flow and

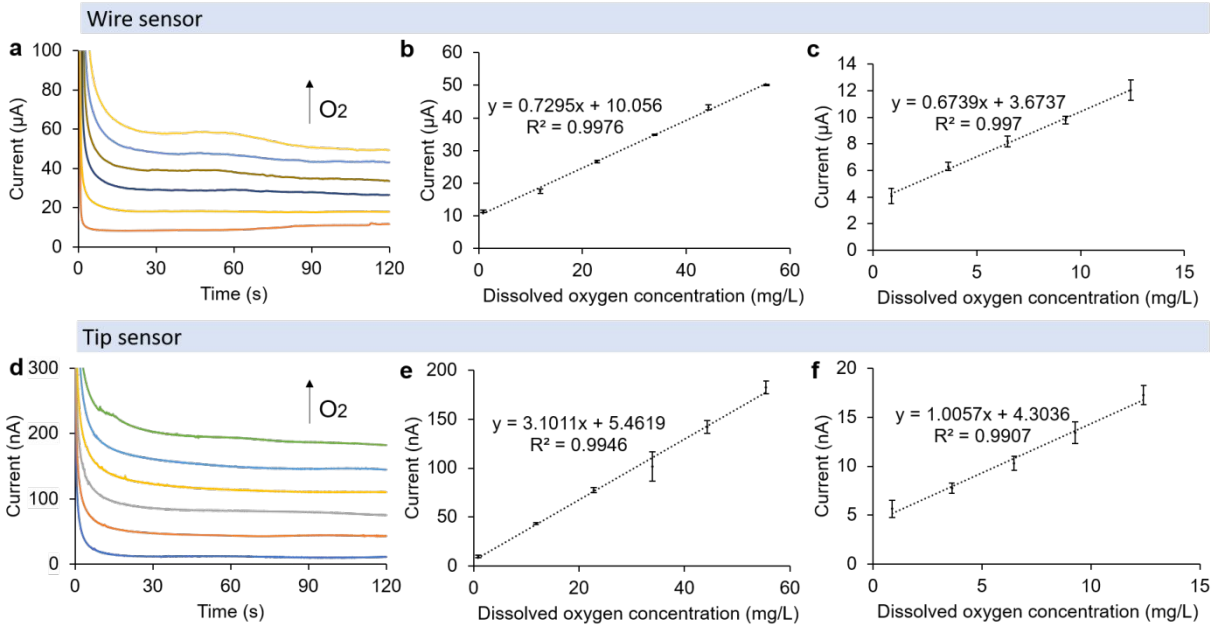

Figure 3. Calibration curve of thread-based oxygen sensor. (a-c) 'Wire' sensor. (d-f) 'Tip' sensor. (a) & (d) Chronoamperometry curves of different dissolved oxygen concentration in PBS. (b) & (e) Calibration plot of the curve in (a) & (d). (c) & (f) Calibration plot in the physiological range. The current value is averaged from the last 30 s from the chronoamperometry curve. Data is represented as mean ± standard deviation.

provides chloride ions for electrode reaction. The electrolyte solution is separated from the external environment using a gas diffusion barrier.[22] In our design the thread electrodes are directly exposed to the external environment hence it's critical to evaluate whether the sensor can function in the tissue environment. We tested sensor's performance in PBS since it has a similar ionic strength and concentration of chloride ion to that of biological fluids.[35] **Figure 3a&d** show the chronoamperometry measurement of wire and tip sensor in response to different concentrations of dissolved oxygen, respectively. The sensor's response time is within 90s, after which the output currents stabilize. **Figure 3b-c &e-f** show calibration curves of wire and tip sensor in full oxygen range (0-100% oxygen saturated PBS, or 0 - 55.47 mg/L dissolved oxygen) and physiological range (0-21% oxygen saturated PBS, or 0 – 12.42 mg/L dissolved oxygen). The tissue oxygen level is considered to be less than ambient oxygen level (21%) which is covered within the linear range of our sensor.[36, 37] For both types of sensor, a linear response is observed in all concentration ranges. Due to the much larger surface area of wire sensor compared to tip sensor, the recorded current for wire sensor is in the level of microamp while for tip sensor, the current lies in the level of nanoamp. The sensitivity is calculated to be 867.8 ± 87 nA/mg·L^{-1} for wire type sensor and 1.94 ± 0.35 nA/mg·L^{-1} for tip type sensor. The limit of detection (LOD) was calculated using the following equation,

$$LOD = 3.3 \times (\frac{S_y}{S})$$

Where S_y denotes standard deviation of the calibration curve and S denotes slope of the curve. LOD was calculated to be 0.95 mg/mL (0.95 ppm) dissolved oxygen for wire sensor and 1.68 mg/mL (1.68 ppm) dissolved oxygen for tip sensor.

3.3 Repeatability and stability of thread-based oxygen sensor

It is important that the sensor can make consistent measurements during repeated testing. To test the repeatability of the sensor, we measured sensor's response by changing dissolved oxygen concentrations repeatedly using air and nitrogen flow. The results (**Figure 4a&b**) suggest that both types of sensor display good reversibility with the variation less than 10%. The stability of the

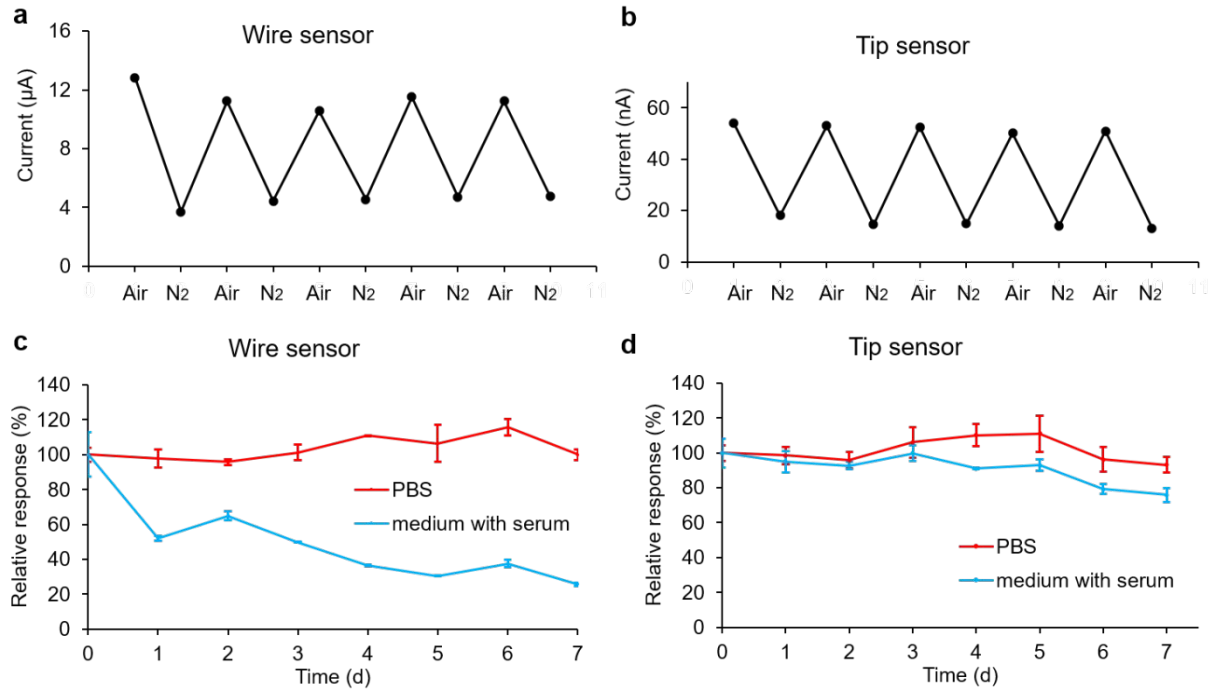

Figure 4. Repeatability and stability test of thread-based oxygen sensor. (a) & (b) Repeatability test of wire and tip type sensor. (c) & (d) Stability test of wire and tip sensor in PBS and medium supplemented with serum. Data is represented as mean ± standard deviation.

sensors was validated by soaking them in PBS (pH 7.4) and DMEM medium supplemented with FBS for 7 days and recording the change of current. In PBS buffer, for both types of sensors, the current was stable over the period of 1 week with the signal variation less than 10% (**Figure 4b&d**). In medium, a gradual decrease in signal is observed for both types of sensor over 7 days. The signal reduction is 74.28 ± 0.91% for wire sensor and 24.05 ± 3.98% for tip sensor at day 7. It should be noted the sensors were still functioning after 7 days soaking in culture medium but with reduced sensitivity. For short-term use, the sensor can still be recalibrated in medium if applied to ex vivo culture system. An antifouling layer is needed to enhance sensor's stability for long term use.[33, 34]

3.4 Interference study

The tissue pH level varies and is associated with physiopathological statues of the local tissue environment. For example, pH value in chronic wounds is found to vary between 5.45 and 8.65.[38] Wound pH could transit from a more acidic state to a more alkaline state when there is an infection.[39] It is therefore important to evaluate the sensor's response at different pH levels. As shown in **Figure 5**, both types of sensor show highly stable response in buffers with pH from 5.8 to 8.0. This is beneficial for probing wound oxygenation as well as measuring oxygen profile in ex vivo cell culture system where pH could fluctuate due to cell metabolism. To test sensor's response in non-ideal fluids, we soaked sensors in cell culture medium and compared their signal with that in the buffers. The signal reduction was 20% for wire sensor and 10% for tip sensor compared with their response in buffers after soaking in medium for 20 min, which was caused by adsorption of serum proteins onto the electrodes as discussed previously (**Figure 5**).

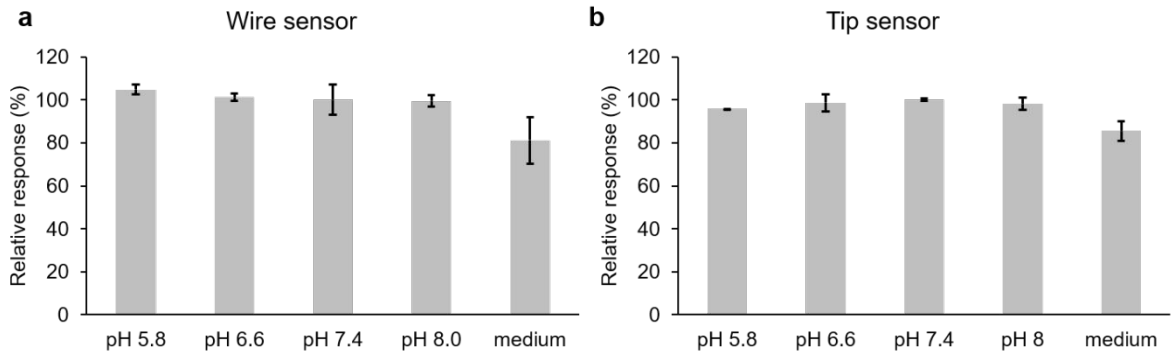

Figure 5. Interference test of thread-based wire (a) and tip (b) oxygen sensor in different pH buffers and cell culture medium. Signal is normalized against pH buffer 7.4. Data is represented as mean ± standard deviation.

3.5 Bending test

To study the effect of mechanical deformation on sensor's performance, deformation test is carried out by physically bending the active sensing zone of wire sensor as shown in **Figure 6a**. The threads are sown to a flexible PET film and submerged in air-saturated PBS buffer with pH of 7.4, while chronoamperometry measurement is conducted before, during, and after (retraction) the bending. The bending direction is perpendicular to the threads to ensure minimum change in

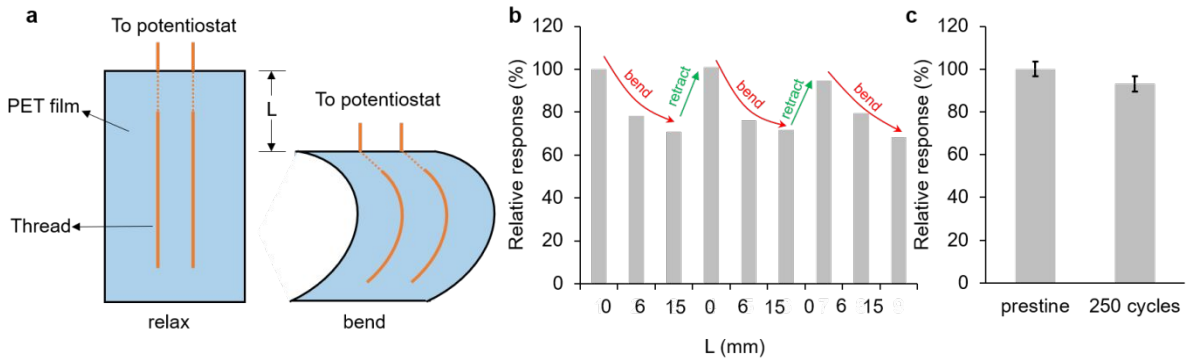

Figure 6. Bending test of thread-based oxygen sensor. (a) Experimental setup. (b) Sensor's response during 3 bending-retraction cycles. (c) Sensor's response after 250 bending cycles. Data is represented as mean ± standard deviation.

spacing between them during bending. The reduction in vertical length of PET sheet caused by bending, L, is used to indicate the degree of bending. **Figure 6b** shows sensor's response during 3 bending cycles. As the sheet was bent by 6 mm, the output signal reduced to 80% of that before bending. Further bending the sheet by 9 mm (total 15 mm) caused another 10% reduction in signal. We speculate the signal reduction could be caused by change in electrode surface area as bending re-arranges positions of individual fiber in the thread. More importantly, the signal was almost fully recovered after the threads were retracted to the original position after each bending cycle. We further conducted 250 continuous bending-retraction cycles. The signal loss was only 6.91 ±2.55% which proves that the sensor is robust enough against mechanical wear and tear when integrated with tissue.

3.6 Tissue model study

A major advantage of thread-based electrochemical sensor is that it harnesses the soft and flexible nature of textile to make it suitable as implantable sensors. As a proof-of-concept, we used agarose gel as a tissue mimic to validate sensor's performance in tissue-like environment. Note that agarose is widely used as a tissue phantom for biomedical applications.[40, 41] In order to establish the oxygen gradient inside the gel, a cylindrical gel was formed inside a tube where its bases are exposed to air and nitrogen flow, respectively. Four individual pre-calibrated tip sensors were inserted from the side to measure oxygen concentration inside the gel at different locations (**Figure 7a**). Due to the geometry of the gel and the diffusion kinetics of oxygen, the oxygen gradient is expected to form along the height direction, where the diffusion zone is close to the boundary with the length of a few millimeter.[42, 43] We observed increased current values with increased distance between the sensor tip and the gel surface exposed to nitrogen, where the signal levels off at ~7 mm, consistent with our expectation (**Figure 7b**). A similar oxygen concentration profile is validated by using the commercial oxygen probe (**Figure S5**). Note that due to the much smaller size of the tip sensor, it possesses higher spatial resolution (more data points per unit distance) compared with the commercial probe. The results also prove that the tip sensor is mechanically stable during insertion into the gel. We envision for clinical application, the thread-based sensor can be implanted into the tissue using a suture needle because of its small size and similar property of a suture thread. For wire type sensor, a second thread needs to be placed alongside as the anode electrode. To simplify the procedure, the anode thread can be bundled together with the cathode sensing thread using dielectric ink as an insulating layer.

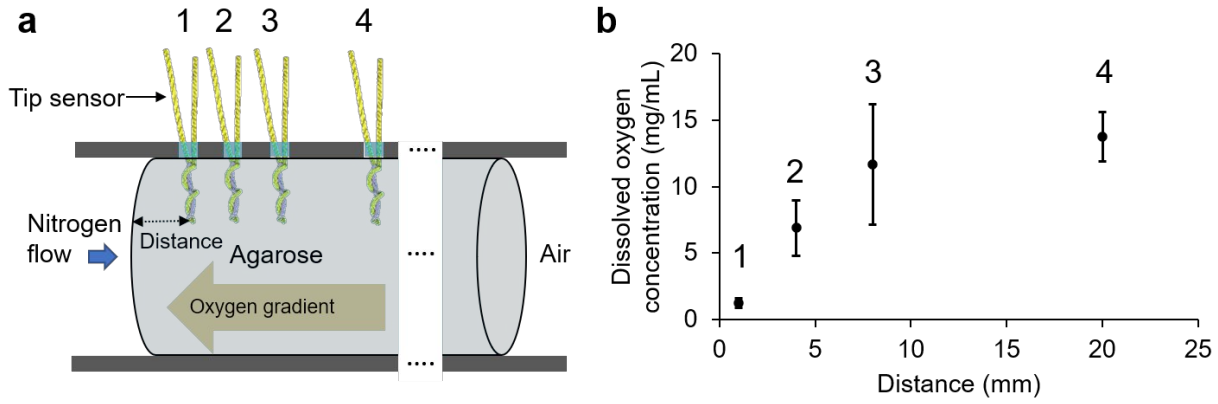

Figure 7. Tissue model study of thread-based oxygen sensor. (a) Experimental setup. (b) Sensor's response in relation to its position inside the gel. The cylindrical agarose gel has a radius of 1.45 cm and a length of 4.5 cm. Data is represented as mean ± standard deviation.

4. Conclusion and future work

In this work we have developed a highly flexible electrochemical oxygen sensor using threads as sensing electrodes for sensitive detection of dissolved oxygen concentration. Specifically, we fabricated a wire and a tip type sensor to measure averaged oxygen concentration over a large area or local oxygen concentration at region of interest. Both types of sensor have a linear range over 0-55.47 mg/L dissolved oxygen and have a LOD around 1 mg/mL (1 ppm). The sensor displays good repeatability and stability in buffer solution over 1 week. Moreover, the sensors are resilient to change in pH and mechanical deformation. Due to its inherent flexibility and sensitivity, such thread-based oxygen sensors can be useful in areas such as wound oxygen monitoring and organ-on-a-chip study where oxygen profile inside 3-D cell constructs is of great interests.[42] As with any tools, there are issues to be addressed in future study. The selectivity of the sensor to other gas species needs to be further tested. Several anti-fouling strategies could be employed, including coating the thread surface with an oxygen-permeable membrane such as PDMS or hydrogel, or using anti-fouling layer made from porous cross-linked bovine serum albumin (BSA).[44] The coating may increase the response time of the sensor since it creates a diffusion barrier, which needs to be investigated in future study. In addition, the bio-compatibility of the sensor should be evaluated for implanted sensors. To make the sensor easy-to-use for point-of-care diagnosis, a miniaturized electronic readout system should be integrated into the sensing platform in the future work similar to our prior work.[45-47]

Author Information

Corresponding Author

Email: sameer@ece.tufts.edu

Author Contributions

The manuscript was written through contributions of all authors. All authors have given approval to the final version of the manuscript.

Notes

The authors declare no competing financial interests.

Acknowledgement

Partial support for the project was provided by DTA Medical and National Science Foundation.

References

1. H. J. Seo, W. M. Bahk, T. Y. Jun and J. H. Chae, *Clinical Psychopharmacology and Neuroscience*, 2007, **5**, 25-30.
2. H. S. Kim, M. H. Choi, J. H. Baek, S. J. Park, J. C. Lee, U. H. Jeong, S. P. Kim, H. J. Kim, Y. Choi, D. W. Lim and S. C. Chung, *J Physiol Anthropol*, 2015, **34**, 3.
3. F. Gottrup, *World J Surg*, 2004, **28**, 312-315.
4. S. Schreml, R. M. Szeimies, L. Prantl, S. Karrer, M. Landthaler and P. Babilas, *Br J Dermatol*, 2010, **163**, 257-268.
5. T. V. Veenith, E. L. Carter, T. Geeraerts, J. Grossac, V. F. Newcombe, J. Outtrim, G. S. Gee, V. Lupson, R. Smith, F. I. Aigbirhio, T. D. Fryer, Y. T. Hong, D. K. Menon and J. P. Coles, *JAMA Neurol*, 2016, **73**, 542-550.
6. B. Muz, P. de la Puente, F. Azab and A. K. Azab, *Hypoxia (Auckl)*, 2015, **3**, 83-92.
7. F. J. Giordano, *Journal of Clinical Investigation*, 2005, **115**, 500-508.
8. D. A. Boas and M. A. Franceschini, *Philos Trans A Math Phys Eng Sci*, 2011, **369**, 4407-4424.
9. K. K. Tremper and S. J. Barker, *Anesthesiology*, 1989, **70**, 98-108.
10. J. Liu, Y. Liu, W. Bu, J. Bu, Y. Sun, J. Du and J. Shi, *J Am Chem Soc*, 2014, **136**, 9701-9709.
11. X. Zheng, X. Wang, H. Mao, W. Wu, B. Liu and X. Jiang, *Nat Commun*, 2015, **6**, 5834.
12. Y. Khan, D. Han, A. Pierre, J. Ting, X. Wang, C. M. Lochner, G. Bovo, N. Yaacobi-Gross, C. Newsome, R. Wilson and A. C. Arias, *Proc Natl Acad Sci U S A*, 2018, **115**, E11015-E11024.
13. M. Ochoa, R. Rahimi, J. Zhou, H. Jiang, C. K. Yoon, D. Maddipatla, B. B. Narakathu, V. Jain, M. M. Oscai, T. J. Morken, R. H. Oliveira, G. L. Campana, O. W. Cummings, M. A. Zieger, R. Sood, M. Z. Atashbar and B. Ziaie, *Microsystems & Nanoengineering*, 2020, **6**.
14. N. A. Wisniewski, S. P. Nichols, S. J. Gamsey, S. Pullins, K. Y. Au-Yeung, B. Klitzman and K. L. Helton, *Adv Exp Med Biol*, 2017, **977**, 377-383.
15. A. Stekelenburg, D. Gawlitta, D. L. Bader and C. W. Oomens, *Arch Phys Med Rehabil*, 2008, **89**, 1410-1413.
16. J. Ehgartner, H. Wiltsche, S. M. Borisov and T. Mayr, *Analyst*, 2014, **139**, 4924-4933.
17. R. Li, H. Qi, Y. Ma, Y. Deng, S. Liu, Y. Jie, J. Jing, J. He, X. Zhang, L. Wheatley, C. Huang, X. Sheng, M. Zhang and L. Yin, *Nat Commun*, 2020, **11**, 3207.
18. C. Liu, Y. Zhao, X. Cai, Y. Xie, T. Wang, D. Cheng, L. Li, R. Li, Y. Deng, H. Ding, G. Lv, G. Zhao, L. Liu, G. Zou, M. Feng, Q. Sun, L. Yin and X. Sheng, *Microsystems & Nanoengineering*, 2020, **6**.
19. W. J. Whalen, J. Riley and P. Nair, *J. Appl. Physiol.*, 1967, **23**, 798–801.
20. J. M. Lash and H. G. Bohlen, *Am. J. Physiol.*, 1987, **252**, H1192–1202.
21. B. R. Duling and R. M. Berne, *Circ. Res.*, 1970, **27**, 669-678.
22. L. C. Clark, R. Wolf, D. Granger and Z. Taylor, *J. Appl. Physiol.*, 1953, **6**, 189-193.
23. K. Jonsson, J. A. Jensen, W. H. Goodson, H. Scheuenstuhl, J. West, H. W. Hopf and T. K. Hunt, *Ann. Surg.*, 1991, **214**, 605-613.
24. G. Acar, O. Ozturk, A. J. Golparvar, T. A. Elboshra, K. Böhringer and M. K. Yapici, *Electronics*, 2019, **8**.
25. A. Hatamie, S. Angizi, S. Kumar, C. M. Pandey, A. Simchi, M. Willander and B. D. Malhotra, *Journal of The Electrochemical Society*, 2020, **167**.
26. M. Stoppa and A. Chiolerio, *Sensors (Basel)*, 2014, **14**, 11957-11992.
27. P. Mostafalu, M. Akbari, K. A. Alberti, Q. Xu, A. Khademhosseini and S. R. Sonkusale, *Microsyst Nanoeng*, 2016, **2**, 16039.
28. P. Mostafalu, A. Tamayol, R. Rahimi, M. Ochoa, A. Khalilpour, G. Kiaee, I. K. Yazdi, S. Bagherifard, M. R. Dokmeci, B. Ziaie, S. R. Sonkusale and A. Khademhosseini, *Small*, 2018, DOI: 10.1002/smll.201703509, e1703509.
29. T. Terse-Thakoor, M. Punjiya, Z. Matharu, B. Lyu, M. Ahmad, G. E. Giles, R. Owyeung, F. Alaimo, M. Shojaei Baghini, T. T. Brunyé and S. Sonkusale, *npj Flexible Electronics*, 2020, **4**.

30. D. W. Kinsey and R. A. Bottomley, *J. Inst. Brew*, 1962, **69**, 164-176.
31. D. H. Phillipst and M. J. Johnson, *J. Biochem. Microbiol. Technol. Engng*, 1961, **3**, 261-275.
32. Y. Mendelson, 2012, **Chapter 10 - Biomedical Sensors**, 609-666.
33. S. Li, J. Dai, M. Zhu, N. Arroyo-Currás, H. Li, Y. Wang, Q. Wang, X. Lou, T. E. Kippin, S. Wang, K. W. Plaxco, H. Li and F. Xia, *bioRxiv*, 2020, **doi: https://doi.org/10.1101/2020.11.15.383992**.
34. B. Yu, C. Wang, Y. M. Ju, L. West, J. Harmon, Y. Moussy and F. Moussy, *Biosens Bioelectron*, 2008, **23**, 1278-1284.
35. B. Chazotte, *Cold Spring Harb Protoc*, 2012, **2012**.
36. S. R. McKeown, *Br J Radiol*, 2014, **87**, 20130676.
37. S. M. Evans, A. E. Schrlau, A. A. Chalian, P. Zhang and C. J. Koch, *J Invest Dermatol*, 2006, **126**, 2596-2606.
38. J. Dissemond, M. Witthoff, T. C. Brauns, D. Haberer and M. Goos, *Hautarzt*, 2003, **54**, 959-965.
39. S. L. Percival, S. McCarty, J. A. Hunt and E. J. Woods, *Wound Repair Regen*, 2014, **22**, 174-186.
40. A. D. Maxwell, T. Y. Wang, L. Yuan, A. P. Duryea, Z. Xu and C. A. Cain, *Ultrasound Med Biol*, 2010, **36**, 2132-2143.
41. M. D. Mitchell, B. A. Harold, L. Kundel, L. Axel and P. M. Joseph, *Magnetic Resonam Imaging*, 1986, **4**, 263-266.
42. H. Zirath, M. Rothbauer, S. Spitz, B. Bachmann, C. Jordan, B. Muller, J. Ehgartner, E. Priglinger, S. Muhleder, H. Redl, W. Holnthoner, M. Harasek, T. Mayr and P. Ertl, *Front Physiol*, 2018, **9**, 815.
43. R. L. Wilson, J. P. Connell and K. J. Grande-Allen, *ACS Biomaterials Science & Engineering*, 2019, **5**, 4522-4530.
44. J. Sabate Del Rio, O. Y. F. Henry, P. Jolly and D. E. Ingber, *Nat Nanotechnol*, 2019, **14**, 1143-1149.
45. P. Mostafalu, W. Lenk, M. R. Dokmeci, B. Ziaie, A. Khademhosseini and S. R. Sonkusale, *IEEE Trans Biomed Circuits Syst*, 2015, **9**, 670-677.
46. M. Punjiya, P. Mostafalu and S. Sonkusale, *2014 IEEE Biomedical Circuits and Systems Conference (BioCAS) Proceedings*, 2014.
47. M. Punjiya, C. H. Moon, Z. Matharu, H. Rezaei Nejad and S. Sonkusale, *Analyst*, 2018, **143**, 1059-1064.